Quantitative Measurements of Apoptotic Cell Properties Using Acoustic Microscopy

Eric M. Strohm, Gregory J. Czarnota, and Michael C. Kolios

***Abstract*—Time-resolved acoustic microscopy was used to measure properties of cells such as the thickness, sound velocity, acoustic impedance, density, bulk modulus, and attenuation, before and after apoptosis. A total of 12 cells were measured, 5 apoptotic and 7 non-apoptotic. Measurements made at 375 MHz showed a statistically significant increase in the cell thickness from 13.6 ± 3.1 μm to 17.3 ± 1.6 μm, and in the attenuation from 1.08 ± 0.21 dB/cm/MHz to 1.74 ± 0.36 dB/cm/MHz. The other parameters, such as the sound velocity, density, acoustic impedance, and bulk modulus remained similar within experimental error. Acoustic images obtained at 1.0 GHz showed increased RF-signal backscatter and a clear delineation of the nucleus and cytoplasm from apoptotic cells compared with non-apoptotic cells. Extensive activity was observed optically and acoustically within apoptotic cells. Acoustic measurements made one minute apart showed variations in the ultrasonic backscatter but not attenuation in the cells, which indicated rapid structural changes were occurring but not changes in bulk composition. The normalized cross-correlation coefficient was used to quantify the variations in the backscatter RF-signal during apoptosis by comparing the first RF signal measured to each successive RF signal every 10 s. A coefficient of 1 indicates strong correlation, whereas a coefficient of 0 indicates no correlation. An average correlation coefficient of 0.93 ± 0.05 was measured for non-apoptotic cells, compared with 0.68 ± 0.17 for apoptotic cells, indicating that the RF signal as a function of time varied rapidly during apoptosis.**

I. Introduction

Apoptosis, or programmed cell death, is a controlled method of cellular disassembly designed to minimize disruption and damage to surrounding tissue [1], [2]. It is thought to be an integral part in the response of tumors to chemotherapeutic treatment [3], [4], but is also involved in other biological functions such as homeostasis [5], [6], embryonic development [7], and lymphocyte development [8].

Deregulation of apoptosis is present in a variety of diseases, such as Alzhiemer's and AIDS, and inhibition of apoptosis can result in autoimmune disorders and tumors [9]. Several cancerous tumors grow because of a mutation that prevents apoptosis from occurring. Therefore the study of apoptosis is critical to understanding cancer growth and formulating treatments for this disease [10]. How cellular properties change during apoptosis, such as the thickness, density, speed of sound, acoustic impedance, bulk modulus, and their attenuation of sound is not understood. A high-resolution noninvasive technique would assist in the measurement of these properties.

Measurement of the acoustic properties of cells is not trivial. Techniques such as microrheology [11], magnetic twisting cytometry [12], micropipette aspiration [13], microneedle investigations [14], optical [15] and magnetic tweezer studies [16], and atomic force microscopy [17] are invasive and/or require direct contact with the cell, which may alter cellular properties during the measurement. Additionally, these methods generally measure bulk properties in cells, and may not be able to measure rapid cellular changes during certain biological processes such as apoptosis.

Ultrasound is non-invasive and can be used to determine the qualitative and quantitative properties of cells and bulk tissue without staining or fixation. Previous studies using high-frequency (HF) ultrasound (20 to 60 MHz) reported an increase in the ultrasound backscatter intensity for cells treated with chemotherapeutic drugs to induce apoptosis compared with untreated cells, and also changes in the frequency dependence of the ultrasound scattering [18]–[21]. It was hypothesized that the structural changes within apoptotic cells were responsible for the increase in backscatter observed [22]. However, the source of increased backscatter could also be due, in part, to changes in the spatial rearrangement of cellular and sub-cellular structures responsible for the scattered sound [23]. The source of the increased backscatter intensity cannot be easily determined using HF ultrasound alone because of the relatively large wavelength of the sound compared with the cell size (15 to 30 μm). Therefore, additional studies must be performed. A key to understanding these observations with HF ultrasound requires knowledge of the acoustical properties of the cell. These properties can change during various physiological processes such as apoptosis, mitosis, locomotion, and adhesion. Cell mechanical property changes as a function of time for these processes is poorly understood [24], [25].

Acoustic microscopy is capable of resolving individual cells and organelles using frequencies of 100 to 1000 MHz [26], for which the resolution approaches 1 μm at 1 GHz. Ultrasound can be used to measure the properties of cells

Manuscript received November 27, 2009; accepted June 8, 2010. This research was undertaken, in part, thanks to funding from the Canada Research Chairs Program awarded to M. C. Kolios. Funding to purchase the equipment was provided by the Canada Foundation for Innovation, the Ontario Ministry of Research and Innovation, and Ryerson University. G. J. Czarnota is supported through a Cancer Care Ontario Research Chair in Experimental Therapeutics and Imaging and Sunnybrook Health Sciences Centre.

E. M. Strohm and M. C. Kolios are with the Department of Physics, Ryerson University, Toronto, ON, Canada (e-mail: mkolios@ryerson.ca).

G. J. Czarnota is with the Departments of Radiation Oncology and Imaging Research, Sunnybrook Health Sciences Centre, and the Departments of Radiation Oncology and Medical Biophysics, University of Toronto, Toronto, ON, Canada.

Digital Object Identifier 10.1109/TUFFC.2010.1690

and tissue non-invasively and can be localized to specific regions of interest. Although unsuitable for clinical studies because of the limited penetration depth, acoustic microscopy is ideal for measuring the acoustical properties from individual cells [27]–[34] and thin tissue sections [35]–[38]. However, only recently were the thickness, sound velocity, acoustic impedance, density, bulk modulus, and attenuation of live single cells measured together with one technique based on the same data set [39]. It is important to acquire the data with one technique over the same cellular location based on the same RF data when there are rapid temporal variations in the properties of cells. These cell properties can provide insight in the phenomenon observed using HF ultrasound and can be used in computer modeling and simulations to help understand ultrasound scattering and attenuation during the apoptotic process as well as the imaging of bulk tissue at high frequencies [40]–[42].

Recent advancements in technology have enabled recording of the RF-pulse as a function of time at high sampling frequencies in the gigahertz range. Short pulses combined with an increased SNR from post-processing methods have allowed for time-resolved measurements, in which the backscatter echoes from the cell and substrate can now be separately resolved. This is a significant advancement over other acoustic microscopy methods in that the mechanical properties can be directly obtained with a single measurement [43]. Biological specimens present additional difficulties over isotropic and homogenous inorganic solids, as they are complex organisms made up of many components which can be time variant and which respond to external stimuli. In typical acoustic microscope systems, it is not possible to optically view the sample while measurements are made; therefore, it is impossible to know exactly what has been imaged. The acoustic microscope used in this research has the capability of simultaneous optical and acoustic measurements, a distinct advantage over other microscope systems. Details of the acoustic microscope can be found elsewhere [29]. In this paper, acoustic microscopy is used to probe, with high spatial resolution, the mechanical properties of cells that have been exposed to chemotherapeutics that induced apoptosis. Moreover, rapid temporal measurements are made of cells responding and not responding to the treatment to examine how ultrasonic properties change as a function of time during apoptosis. A method is presented to extract the mechanical and acoustical properties of interest, and this method is validated by comparing the values measured to those of materials with known properties. This method is then applied to the cell data for quantitative measurements. We present the first reported qualitative and quantitative measurements of the mechanical and acoustical properties of cells during apoptosis.

II. Theory—Acoustic Microscopy

Acoustic microscopy uses ultrasound scattered from the cell membrane and the substrate to determine the ultrasonic properties of cells. The ultrasound pulses must be short enough so that the interface echoes are separated in time. A typical acoustic microscopy setup is shown in Fig. 1, with the transducer positioned above the cell. Pulse echoes from the cell (t_1) and cell-substrate (t_2) are recorded as a function of time (Fig. 2). A reference measurement (t_0) is then made by moving the transducer beside the cell and measuring the pulse echo from the substrate only.

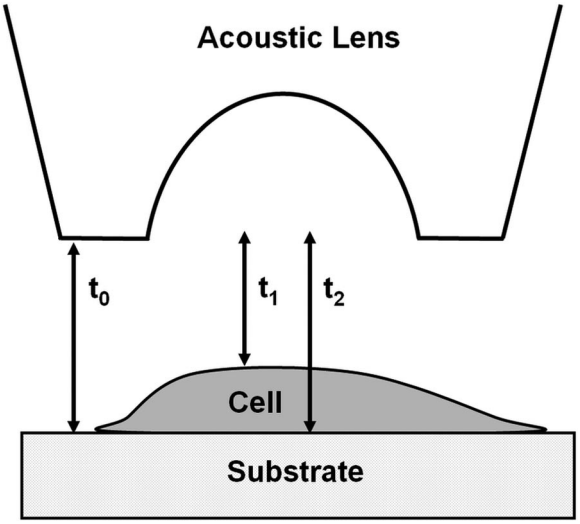

Fig. 1. A schematic of the acoustic microscope experimental setup. The acoustic lens was positioned at a specific distance above the cell. The time-of-flight of the ultrasound backscatter t_0, t_1, and t_2 from the substrate, surface of the cell, and cell-substrate interface, respectively, are used in quantitative calculations of the properties of cells. The pulse-echoes from the cell are measured first, then the transducer is moved to a region beside the cell to measure the reference signal, as indicated by the arrow at t_0.

The mechanical property calculations were completed using established methods [44]. The thickness, d, and the sound velocity, c, of the cell can be calculated using time-resolved methods. The time of the echoes from the top of the cell, t_1, the substrate-cell interface, t_2, and a reference measurement from the substrate, t_0, are used in the following equations

$$d = \frac{c_0}{2}(t_0 - t_1), \tag{1}$$

$$c = c_0 \frac{t_0 - t_1}{t_2 - t_1}, \tag{2}$$

where c_0 is the sound velocity in the coupling fluid.

$V(z)$ measurements, where the signal is recorded as a function of axial position through the cell [45]–[48], are used to determine the remaining ultrasonic properties. The $V(z)$ measurement is made to determine the maximum signal amplitude from each interface, A_1, A_2, and A_3 from the cell surface, cell-substrate interface, and substrate, respectively (Fig. 3). The amplitude of the incident signal A_0 is required and can be found using

$$A_0 = A_3 \frac{Z_s + Z_0}{Z_s - Z_0}, \tag{3}$$

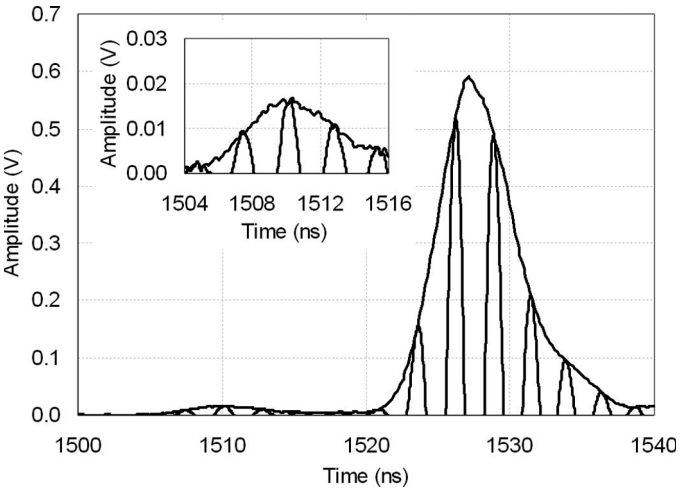

Fig. 2. The positive portion of an ultrasound backscatter signal (and the envelope determined by using a Hilbert transform) from a non-apoptotic cell is plotted as a function of time. The first echo is from the cell membrane, the second is from the cell-substrate interface. Inset: A rescaled view showing the backscatter from the cell membrane.

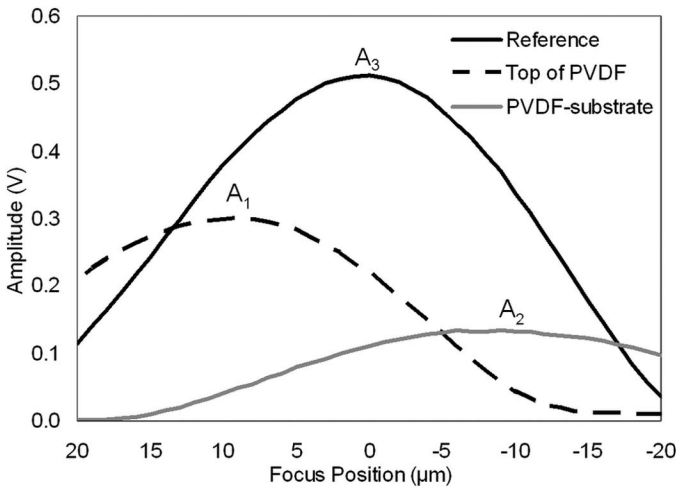

Fig. 3. $V(z)$ curves showing the maximum RF-signal as a function of axial focus position through PVDF, at a probing frequency of 375 MHz. The maximum amplitudes A_1, A_2, and A_3 of the PVDF surface, PVDF-substrate interface, and substrate, respectively, are used to determine the acoustic impedance of the PVDF.

where Z_s and Z_0 are the known acoustic impedances of the substrate and coupling fluid, respectively [49]. The cell acoustic impedance can then be calculated from

$$Z = Z_0 \frac{A_0 + A_1}{A_0 - A_1}. \tag{4}$$

Using the sound velocity calculated from the time-resolved methods and the acoustic impedance calculated from the $V(z)$ methods, the density ρ, and bulk modulus K can be calculated using

$$\rho = \frac{Z}{c}, \tag{5}$$

$$K = cZ = \rho c^2. \tag{6}$$

Finally, the attenuation can be calculated using

$$\alpha = \alpha_c + \frac{1}{2d}\left[\frac{A_3}{A_2}\frac{Z_s - Z}{Z_s + Z}\frac{4ZZ_0}{\left(Z + Z_0\right)^2}\frac{Z_s + Z_0}{Z_s - Z_0}\right], \tag{7}$$

where α_c is the attenuation calculated through a distance $2d$ in the coupling fluid [44]. The attenuation coefficient α_0 can be calculated using

$$\alpha = \alpha_0 f^n, \tag{8}$$

where n generally varies from 0.9 to 1.2 for bulk tissue [50]. The value of n is not known for individual cells at this frequency range, as bulk tissue contains capillaries, blood and other types of cells which may affect the bulk tissue measurement. In this study, it was assumed that $n = 1$.

Changes in the RF signal measured over time can be quantified by calculating the cross-correlation coefficient. Given two signals x, y, the correlation coefficient between these two signals can be calculated using

$$R_{xy}(m) = \sum_{k}^{N} y(k)x(k+m), \tag{9}$$

where N is the length of the signal [51]. A correlation coefficient of 1 indicates similarity between the two signals, whereas a coefficient of 0 indicates no correlation.

III. Materials and Methods

A. Polyvinylidene Fluoride

The methodology for the measurement of the acoustic properties was verified using a 9-μm-thick PVDF (polyvinylidene fluoride) from Measurement Specialties (Hampton, VA). This material was chosen as its thickness is similar to that of cells and the properties of PVDF have been well studied [52]. The properties of the PVDF were provided by the company (see Table I) [53].

The PVDF was attached to glass slides (Fisher Scientific, Ottawa, Canada) during measurements. The PVDF material must come in contact with the substrate, without air or water pockets for an accurate quantitative measurement. Gently pressing the PVDF onto the substrate proved to be the best method to ensure contact. The PVDF film and the glass surface are held together by the capillary force. Other methods such as gluing the PVDF to the substrate, which added a non-negligible thickness layer, and weighing the sample down with external weights, gave inaccurate results.

Once the PVDF was pressed onto the substrate, it was optically examined for adherence. Thin film interference such as observed in Newton's rings provided an optical

TABLE I. PVDF CALIBRATION RESULTS.

Property	Given value [53]	Calculated value	Percent error
Thickness (μm)	9	8.6 ± 0.4	4.4%
Sound velocity (m/s)	2200	2211 ± 59	0.5%
Acoustic impedance (MRayls)	3.92	3.95 ± 0.09	0.6%
Density (kg/m^3)	1780	1786 ± 80	0.3%
Bulk modulus (GPa)	8.5	8.7 ± 0.2	2.5%
Attenuation (dB/cm per MHz)	—	6.9 ± 1.9	—

A comparison of the calculated values for the mechanical properties of PVDF to the values given by the manufacturer. The standard deviations using five measurements are shown in the calculated values. The percent errors between the calculated and given values are 4.4% or less.

method to ensure that the PVDF was properly adhered to the substrate. The distance between fringes indicated the distance between the PVDF and substrate. Locations with fringes close together were avoided, because this indicated a non-negligible thickness of an air layer beneath the PVDF (Fig. 4).

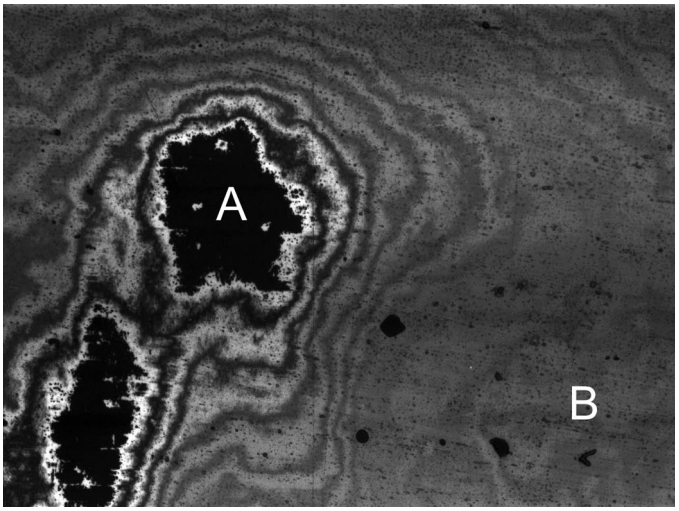

Fig. 4. An optical view of PVDF pressed onto a glass substrate. Interference fringes (near A) were used to determine optimum positions for measurements. At position A, the fringes are closer together indicating there is a non-negligible distance between the substrate and PVDF. In position B, the fringes are far apart, indicating the PVDF and substrate are close enough to prevent the formation of interference rings.

B. Cells

MCF-7 breast cancer cells (ATCC, Manassas, VA) were cultured using Dulbecco's modified Eagle's medium (DMEM) cell culture medium (ATCC) with 10% fetal bovine serum (FBS) and 0.1% insulin. Cells were incubated at 37°C with 5% CO_2 and were passaged every 3 d to maintain exponential growth. Prior to experimentation, cells were dissociated using trypsin and transferred to Lab-Tek II chambers (Nunc, Langenselbold, Germany). After 48 h, in which the cells were allowed to properly adhere to the substrate, the cell culture medium was replaced with a solution consisting of the DMEM cell culture medium (without FBS or insulin), 3 mg/mL caffeine and 20 ng/mL paclitaxel to induce apoptosis [54]–[56]. The cells were allowed to incubate overnight (15 to 20 h) before experimentation at 37°C with 5% CO_2. The entire microscope was enclosed in a climate controlled box to maintain a constant temperature of 36°C ± 0.02°C with 5% CO_2 during experimentation.

C. Acoustic Microscope

The SASAM 1000 acoustic microscope (Kibero GmbH, Saarbrücken, Germany) was used in this experiment. It combines an Olympus IX81 inverted optical microscope with an acoustic module, allowing simultaneous acoustic and optical imaging, including fluorescent imaging. The acoustic module rotates on a column above the sample, and can be switched with an optical condenser allowing for phase contrast imaging before and after acoustic measurements [29], [57].

Two monocycle pulse generators, one at 300 MHz and the other at 1 GHz, each with 100% bandwidth were used to generate the ultrasound pulses with a 10 V_{pp} amplitude and a pulse repetition rate of 500 kHz. Two transducers were used in these experiments. A 375-MHz transducer with a semi-aperture angle of 30° and a −6 dB bandwidth of 42% was used for the quantitative analysis, and a 1.0-GHz transducer with a semi-aperture angle of 50° and a −6dB bandwidth of 29% was used for high-resolution imaging. The theoretical lateral FWHM beam width of these transducers is 4.0 μm (375 MHz) and 1.0 μm (1.0 GHz) [44]. Although the 1.0-GHz transducer provides better resolution, it was unsuitable for mechanical property calculations because the depth of field was too short to resolve the pulse echoes from the cell membrane and substrate during one RF measurement. Fig. 5 shows the Fourier spectra of the pulse echoes from the 375-MHz and 1.0-GHz transducers, measured from a glass substrate.

The transducer was scanned over the surface of the sample in the x, y, z direction using a piezoelectric controller (Piezosystem Jena GmbH, Jena, Germany). The transducer was scanned with step sizes from 0.1 to 2 μm. Shorter step sizes resulted in a higher resolution image at the expense of imaging time. The RF signal recorded at each position was amplified by a 40-dB amplifier and digitized at a rate of 8 GHz. The SNR was increased by averaging 400 RF-lines at 375 MHz, and 1000 RF-lines at 1.0 GHz. A FM-radio band stop filter (88 to 108 MHz) was used to remove noise, and a high-pass filter set at 300 MHz was used during the 1.0-GHz scans. Reference signals of the background were recorded and removed during post processing.

D. Methodology Verification Measurements

Polyvinylidene fluoride (PVDF) is a piezoelectric thermoplastic commonly used to make transducers operating over 15 MHz [52]. The properties of PVDF have been well studied since its first use in 1969 [58], and it can be made

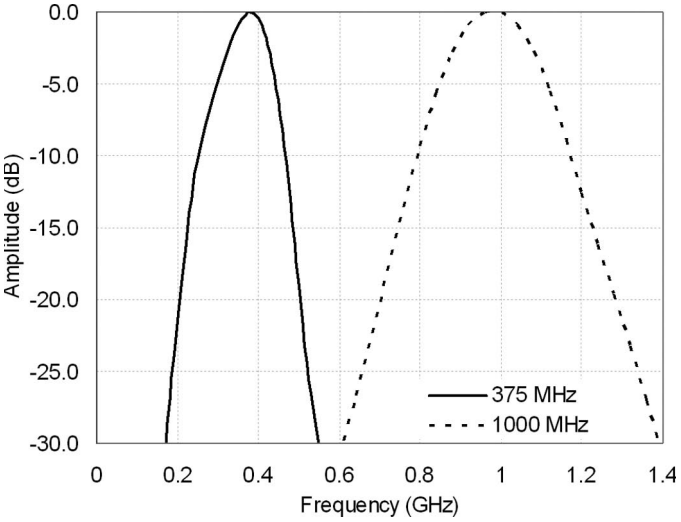

Fig. 5. The Fourier spectra of the pulse echoes from a glass substrate using the 375-MHz and 1.0-GHz transducers. The measurement was made with the focus at the glass substrate.

into very thin films. For these reasons, it makes a suitable material to verify the acoustic microscope methodology.

The PVDF was adhered to a glass slide, and a small amount of water was deposited onto the surface. A $V(z)$ curve measurement was done through the sample, the PVDF pulled from under the transducer, and another $V(z)$ measurement was made to record the reference signal from the substrate. The maximum amplitude of the three interfaces was determined as shown in Fig. 3 and the acoustic impedance of the material was calculated using (3) and (4). The time of the RF-signal from the PVDF surface, PVDF-substrate interface and the substrate were then determined at each z-position in the $V(z)$ curve. The thickness and sound velocity were calculated from the time of the RF-signal echoes t_0, t_1, and t_2 using (1) and (2). Then, the density and bulk modulus were calculated using (5) and (6) and the previously determined acoustic impedance and sound velocity. Finally the attenuation was calculated using (7) and (8).

E. Cellular Measurements

Observations were made to classify cells according to their state, either non-apoptotic and apoptotic. Optical time lapse images were made of an area containing approximately 200 cells for a period of 5 min. Cells that had undergone a morphological change to a spherical shape and showed rapid variations in membrane shape over time were classified as apoptotic. Cells that had maintained their adherent shape, with no membrane blebbing or movement were classified as non-apoptotic. This method of classification worked well for adherent cells because of the difference in shape between apoptotic and non-apoptotic cells.

Once a cell was identified, the transducer was positioned over the cell with the focus at the substrate. The transducer was scanned over the surface of the cell using step sizes from 0.35 to 1.0 μm, recording the RF-signal as a function of time and position. Once the cell was scanned, the focus was changed to 7 μm above the cell (so the focus was approximately in the middle of the cell) and the measurement was repeated. These scans were mainly used to create C-scan images of the cells, and to identify areas of strong backscatter. $V(z)$ curves were then made over the central region of the cell, where the backscatter was typically strongest and membrane curvature was minimized. Step sizes of 1 μm were used, ensuring that both the cell membrane and substrate were recorded during the scan. Once completed, another scan over the surface of the cell was made to ensure the cell didn't move during the scan process. The time required for this process ranged from 5 to 15 min, depending on the step size and resolution used during the scan.

Only the data from the $V(z)$ curves were used for the quantitative calculations. The maximum amplitude was determined from the $V(z)$ curve (Fig. 3), and the time of the RF-signals from the cell membrane and substrate were determined at a slight defocus. These parameters were used to calculate the properties of the cells using (1)–(8). The unpaired t-test was used to compare the mean thickness, sound velocity, acoustic impedance, density, bulk modulus and attenuation of apoptotic and non-apoptotic cells. A p-value of less than 0.05 was considered statistically significant.

Extensive activity was observed in apoptotic cells during visual observations. Morphological variations such as membrane blebbing were clearly visible in real time. Ultrasound was used to examine the interior of the cell and examine the variations that are occurring inside the cell. Optical and acoustic images were made one minute apart of a single cell undergoing apoptosis, with the focus at the substrate. To quantify the activity within a cell, the RF-signal was measured as a function of time from both non-apoptotic and apoptotic cells. The transducer was positioned over the center of a cell and the RF-signal was recorded every 10 s for a period of 900 s. For each cell, the RF-signal was gated to include only the signal from the cell (for example, 1500 to 1520 ns in Fig. 2), then the mean was subtracted for normalization. The cross-correlation coefficient was then calculated at each measurement point using the initial signal measured (time = 0) and each successive RF-signal using (9). A total of eight cells were measured, four apoptotic and four non-apoptotic.

F. Acoustic Imaging Methods

C-scan images were created by integrating the squared a-scan data at each measurement point and assigning the pixel a grayscale value dependent on the integrated intensity. Two types of acoustic images were created from the raster scans. An attenuation image was made by integrating the RF-signal from the substrate only (from 1520 to 1540 ns in Fig. 2), ignoring any signal from the cell. Dark areas denoted strongest attenuation. The other type of image created is based on the cell backscatter only. The

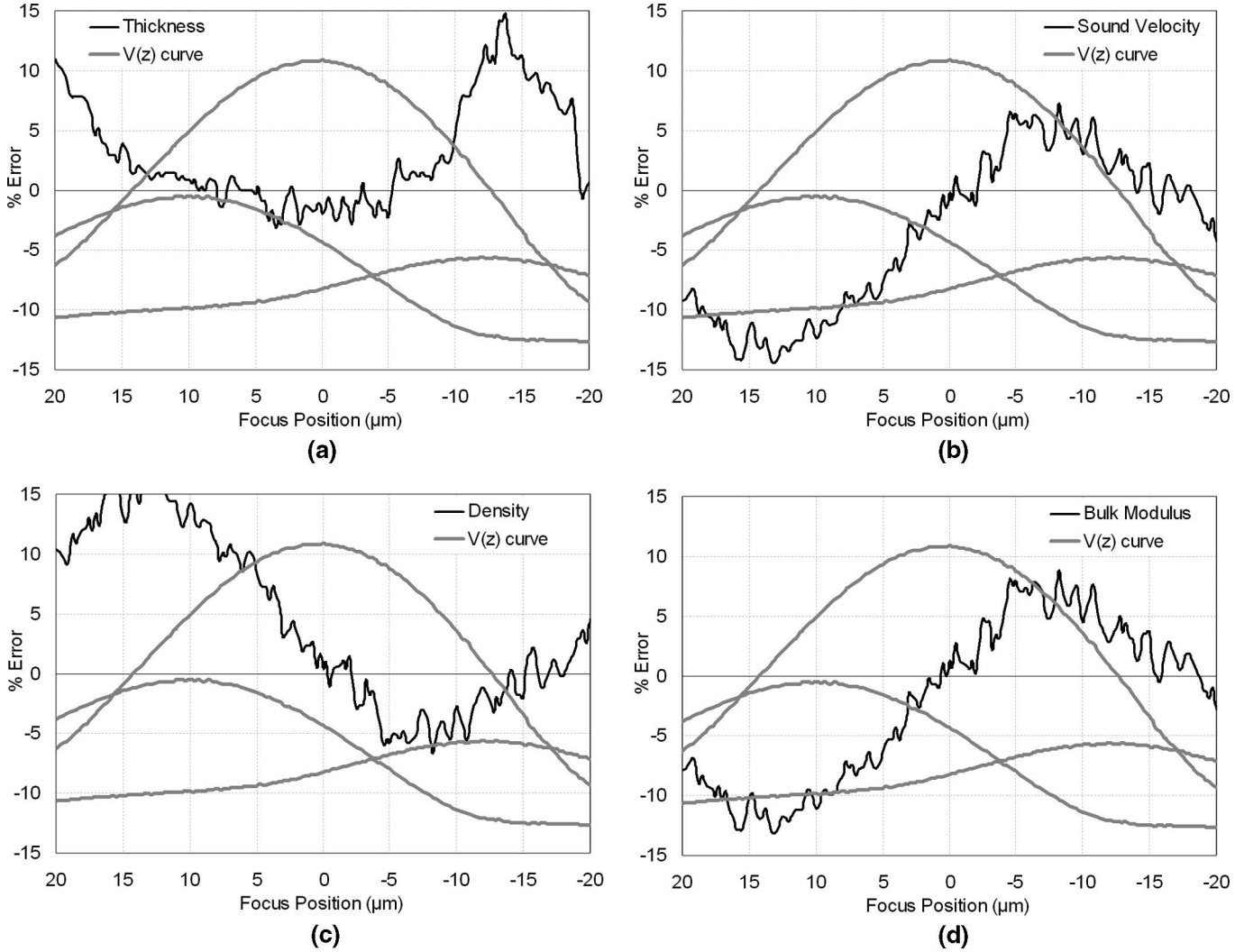

Fig. 6. $V(z)$ curves of PVDF, showing the percent error of the calculated values for the (a) thickness, (b) sound velocity, (c) density, and (d) bulk modulus of the PVDF as compared with the values provided by the manufacturer, overlaid on the graph. The top of the PVDF is to the left (focus position = 10 μm); the bottom of the PVDF to the right (focus position = −12.5 μm).

RF-signal from the cell only is integrated to create the image (1500 to 1520 ns in Fig. 2). Light areas denote strongest backscatter within the cell. These two types of images are useful for showing qualitative cell variations.

IV. Results

A. System Verification

$V(z)$ curves were made through the PVDF sample as discussed in Section III. The PVDF properties, such as the thickness, sound velocity, density, and bulk modulus were calculated at each z-position in the $V(z)$ curve and were compared with the actual values provided by the manufacturer [53]. At each z location, a percent error was calculated between the calculated values and actual values (Fig. 6). The percent error varies according to the z location that the measurements were made. The acoustic impedance is based on the maximum amplitude from the interfaces and therefore does not change with axial position. However, the other calculated parameters vary with axial position. The error for the thickness measurements are minimized in the region from 10 to −5 μm (the substrate focus is at 0 μm), which is roughly between the position of the PVDF surface and surface reference measurement in the axial direction. For the other parameters, the errors are minimized in the region 5 to −5 μm, which is roughly at the axial position of the substrate. The optimum focus location for the thickness calculation was slightly different than the other parameters. Measurements were repeated five times on the same piece of PVDF but at different locations, and the average and standard deviation was calculated, as shown in Table I. The calculated values were compared with the values given by the manufacturer, and a maximum percent error of 4.4% was obtained.

B. Acoustic Images

Acoustic and optical images of treated cells in each state (apoptotic, non-apoptotic) were measured at a frequency of 375 MHz (Fig. 7). The treated, but non-apoptotic cell

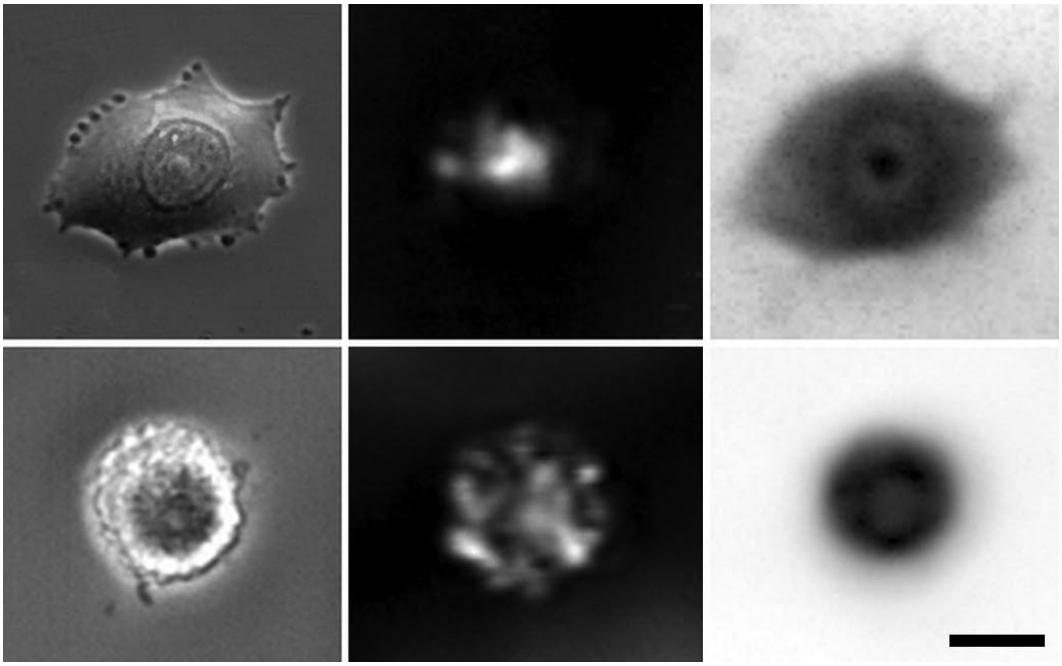

Fig. 7. A comparison of the optical and acoustic images (at 375 MHz) of treated cells: a non-apoptotic cell showing (top) membrane blebbing, an early sign of apoptosis, and (bottom) an apoptotic cell. From left to right: Optical phase contrast images, acoustic c-scan attenuation images, and acoustic c-scan backscatter images. The images shown in this figure are from two different cells. The scale bar is 15 μm.

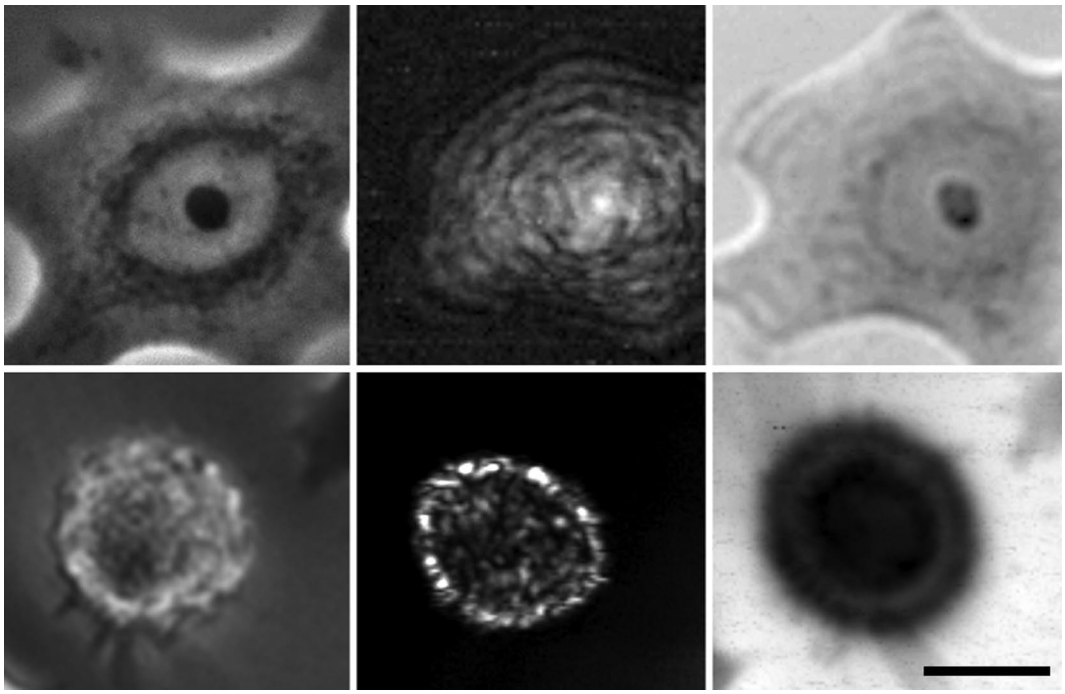

Fig. 8. A comparison of the optical and acoustic images at 1.0 GHz of (top) an untreated cell and (bottom) an apoptotic cell. From left to right: Optical phase contrast images, acoustic backscatter images, and acoustic attenuation images. The images shown in this figure are from two different cells. The scale bar is 15 μm.

showed some initial signs of apoptosis such as blebbing around the cell periphery. At 375 MHz, significant backscatter was observed around the central region of the cell before apoptosis and throughout the entire cell after apoptosis. Untreated and apoptotic cells were also imaged at 1.0 GHz (Fig. 8). The attenuation images clearly show some cellular features such as the cell membrane, nucleus and nucleolus when compared with the optical images. At 1.0 GHz, the nuclear and cytoplasm regions are clearly delineated, and the attenuation in the nucleus appears to be higher than the cytoplasm region. B-mode scans were made of an untreated cell and a treated cell undergoing apoptosis at 1.0 GHz (Fig. 9). The cellular membrane is clearly visible in the untreated cell, whereas the membrane

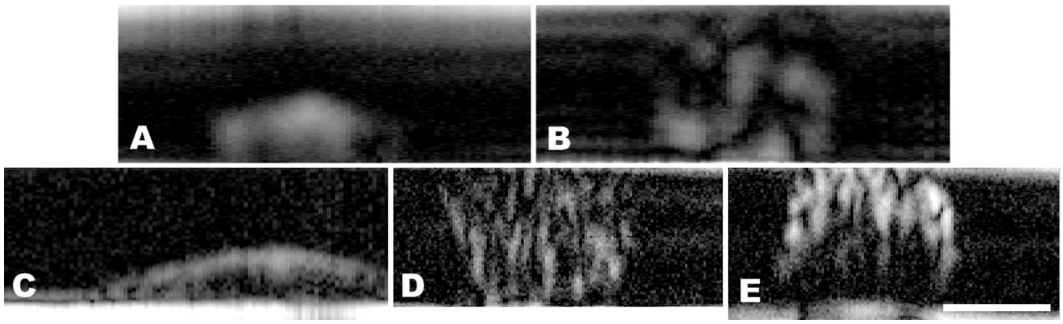

Fig. 9. B-scan images at (top) 375 MHz and (bottom) 1.0 GHz of an untreated cell (A, C) and apoptotic cell (B, D, E). Separate cells were measured at each frequency. The apoptotic B-scan is shown at two different foci at 1.0 GHz: (D) mid-cell and (E) top of the cell. The axial and lateral scales are the same in the images at each frequency. Cell (C) is approximately 7 μm in height, whereas cells (D) and (E) are approximately 18 μm in height. The cellular membrane is clearly visible in the untreated cell, whereas extensive scattering from within the apoptotic cell is observed. The scale bar is 15 μm.

TABLE II. MCF-7 APOPTOSIS MECHANICAL PROPERTY CALCULATIONS.

Property	Non-apoptotic cells	Apoptotic cells
d (μm)	13.6 ± 3.1	17.3 ± 1.6
c (m/s)	1582 ± 19	1574 ± 19
Z (MRayls)	1.56 ± 0.01	1.55 ± 0.02
ρ (kg/m^3)	987 ± 14	984 ± 20
K (GPa)	2.47 ± 0.03	2.44 ± 0.03
α (dB/cm)	405 ± 79	653 ± 135
α (dB/cm per MHz)	1.08 ± 0.21	1.74 ± 0.36

The calculated values and standard deviations of the thickness, sound velocity, acoustic impedance, density, bulk modulus, and attenuation coefficient of apoptotic and non-apoptotic MCF-7 cells.

is less defined for an apoptotic cell. In addition, extensive backscatter from within the apoptotic cell was observed.

C. Ultrasonic Properties

The ultrasonic properties of cells were calculated using the same methodology as for the PVDF verification study. For untreated or non-responding cells, $V(z)$ scans were made around the cell center where the backscatter was generally strongest (Fig. 7). Fig. 2 shows a typical $V(z)$ curve from a treated but non-apoptotic cell, where the RF-signal amplitude from the cell is typically 5 to 25 mV, compared with over 600 mV from the substrate.

In total, 12 cells were measured and C-scans and $V(z)$ curves were completed over 5 apoptotic cells and 7 treated but non-apoptotic cells. A quantitative analysis calculating the thickness, sound velocity, acoustic impedance, density, bulk modulus, and attenuation was completed using the methodology outlined in Section III. The average and standard deviations of cells in both states, treated but non-apoptotic and apoptotic cells, are summarized in Table II.

The thickness of unresponsive cells was 13.6 ± 3.1 μm, compared with 17.3 ± 1.6 μm for responsive cells. The attenuation for unresponsive cells was 1.08 ± 0.21 dB/cm/MHz compared with 1.74 ± 0.36 dB/cm/MHz for responsive cells. The mean thickness and attenuation were statistically different ($p = 0.019$ and 0.010 respectively). The other mechanical properties, including the sound velocity (1582 ± 19 to 1574 ± 19 m/s), acoustic impedance (1.56 ± 0.01 to 1.55 ± 0.02 MRayls), density (987 ± 14 kg/m^3 to 984 ± 20 kg/m^3) and bulk modulus (2.47 ± 0.03 to 2.44 ± 0.03 GPa), were not statistically different ($p = 0.51$, 0.32, 0.79, and 0.14, respectively).

D. Temporal RF-Signal Variations

The variations of the RF-signal from the central region of the cell was investigated by recording the signal from the central region of a cell every 10 s for 900 s. A total of 8 cells were measured, 4 apoptotic and 4 non-apoptotic. The normalized cross-correlation coefficient was calculated using the first RF-signal (time = 0) with each successive RF-signal (Fig. 10). A correlation coefficient of 1 indicates similarity between the two signals, whereas a coefficient of 0 indicates no correlation. Non-apoptotic cells had an average coefficient of 0.93 ± 0.05 and small variations in the correlation coefficient over the measurement period were observed. Apoptotic cells had an average coefficient of 0.68 ± 0.17, and rapid variations were observed.

V. DISCUSSION

A. PVDF Calibration

The methodology outlined in this paper generated a maximum error of 4.4% between PVDF's properties measured at 375 MHz and those provided by the manufacturer (Table I), although the tolerance on the provided values of the PVDF's properties is unknown. Mode conversion did not appear to be an issue at 375 MHz, because of the absence of oscillations in the $V(z)$ curves normally present because of interference with Rayleigh waves. The errors in the methodology verification were too high at 1.0 GHz because of low SNR and poor depth of field, therefore, a quantitative analysis of the properties of cells was restricted to 375 MHz only.

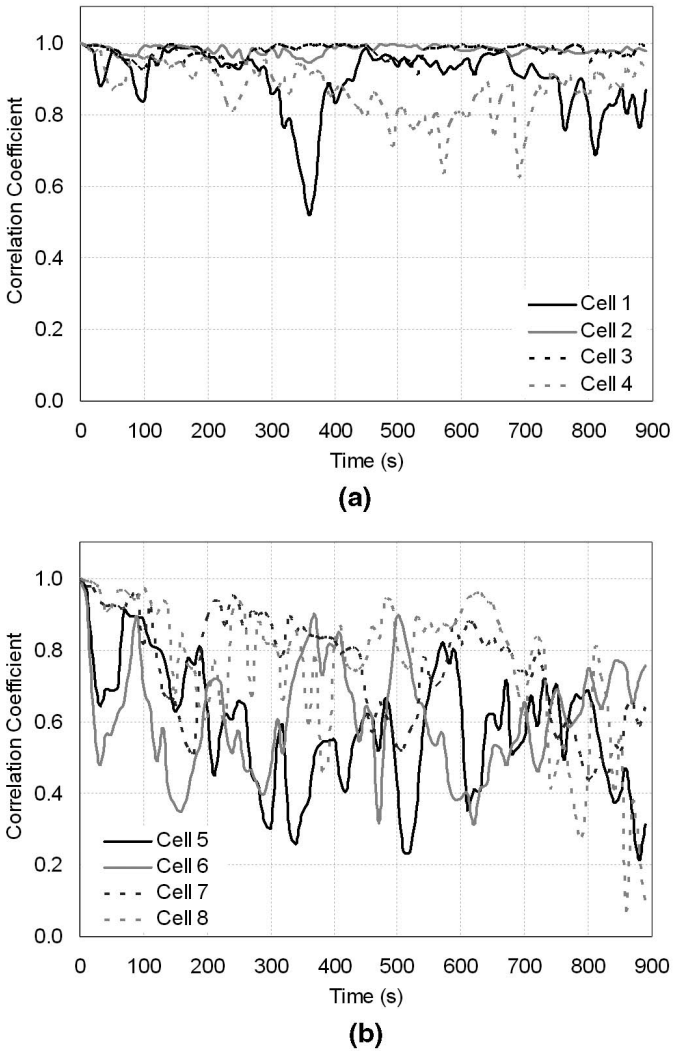

Fig. 10. The stability of the RF-signal over 900 s was determined by calculating the normalized correlation coefficient of the first RF-signal (time = 0) to each successive RF-signal. (A) Four untreated cells, (B) four treated cells undergoing apoptosis.

B. Acoustic Imaging of Apoptosis

Significant backscatter was observed mainly around the center of the cell before apoptosis, and throughout the entire cell after apoptosis. Within the cell, the backscatter intensity from each scattering region before and after apoptosis were similar (the peak voltages measured were generally between 5 and 25 mV). However, the total integrated intensity from the entire cell was larger after apoptosis. This is due to the increase in the number of scattering regions within the cell, as shown in Fig. 7.

The cell membrane was clearly visible at 1.0 GHz for apoptotic and non-apoptotic cells (Fig. 9). However apoptotic cells also had extensive scattering from within the cell, compared with scattering primarily from the cell membrane before apoptosis. Scattering was only observed through the top half of the apoptotic cell [Fig. 9(e)], however this was because the focus was near the cell membrane and the depth of field was only 10 μm using the 1.0-GHz transducer and typical thickness of an apoptotic cell is 15 to 20 μm. When the focus was closer to the substrate, a similar scattering pattern was observed throughout the entire cell [Fig. 9(d)].

The source of scattering could be due to a large number of small scattering structures within the cell that are below the resolving capabilities of this transducer, resulting in a speckle pattern. The scattering was elongated in the axial direction, which would be expected as the axial resolution of the transducer is nearly twice that of the lateral resolution (2.1 μm compared with 1.2 μm) at 1 GHz.

C. Quantitative Calculations

Properties of cells undergoing apoptosis were measured at 375 MHz using acoustic microscopy (Table II). The height of the cells increased by 26% after apoptosis. This is consistent with optical observations, where the cell morphology changes from a flat adherent cell to a spherical shape as the structural proteins within the cell are broken down. It was also found that the attenuation increased by 61% after apoptosis. This increase in attenuation is consistent with the data obtained from HeLa cells undergoing apoptosis [59]. In these experiments, it was shown that the attenuation measured at 1 GHz increased (the measurements were non-quantitative) and attenuation at 20 MHz increased from 0.22 ± 0.05 dB/(MHz·cm) to 0.36 ± 0.07 dB/(MHz·cm). Although it is not known what causes the increase in attenuation, it could be due to cytoplasmic apoptotic bodies formed in early stages, which contain various organelles and fragmented micronuclei which are segregated from the cytoplasm of the apoptotic cell by a shell of microfilaments [60], or other changes induced in this cell line.

The other ultrasonic properties, including the sound velocity, acoustic impedance, density, and bulk modulus, did not change within experimental error during apoptosis. The experimental errors are due to the small sample size and also the intrinsic differences from cell to cell. To reduce the errors in the measurements, a larger sample size could be used. In an effort to examine the active process of apoptosis, only cells with extensive membrane blebbing and activity were measured. Therefore it is possible that the cells measured in this process were all in the early stages of apoptosis. Cells in later stages of apoptosis may have different properties than the early stage, because of the nuclear condensation and breakdown that occur within the cell during apoptosis before splitting into apoptotic bodies. Measurements are in progress to examine the mechanical properties of cells in all stages of apoptosis using the appropriate staining to identify the stages of apoptosis.

It should be noted that the equations used to calculate the acoustical properties of the PVDF, and subsequently the cell, assume a plane wave incident on a planar surface. The large depth of field of the 375 MHz transducer (30 μm), with respect to the size of the objects measured (10 to 20 μm) and the location of the objects in the acous-

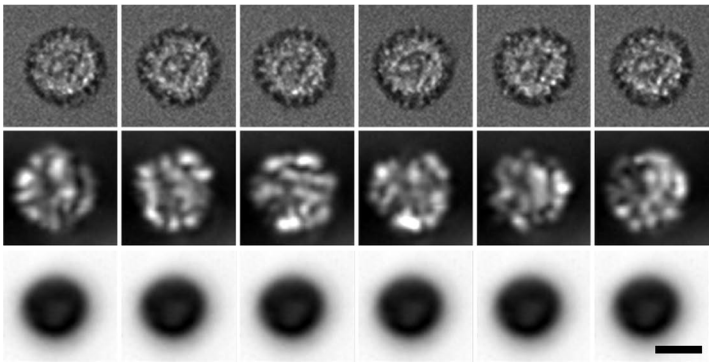

Fig. 11. Optical and acoustic images (at 375 MHz) of an apoptotic cell measured 1 min apart: (top row) optical images, (middle row) acoustic backscatter c-scan images, and (bottom row) acoustic attenuation c-scan images. The attenuation images remained similar during the measurement; however, the optical and acoustic backscatter images show variations over time. The scale bar is 15 μm.

tic beam indicates that the plane wave condition is a good approximation. However, although the PVDF has a planar surface with respect to the incoming acoustic waves, the cell, because of its curvature, is only approximately so. The lateral FWHM of the beam profile for the 375 MHz transducer is 4 μm, and the lateral extent of the cell which is relatively flat varies between 5 and 10 μm depending on whether the cell is apoptotic or not. This is one of the reasons why only the 375 MHz transducer was used in these measurements. Moreover, when the cell property measurements are made, the properties are measured at one location above the cell nucleus, and therefore are representative of the local properties of the interface at that region. Despite these limitations, reasonable values were calculated for the PVDF properties of interest when compared with published values (Table I).

D. Temporal RF-Signal Variations

The rapid morphological changes observed during apoptosis were measured and quantified using acoustic microscopy. Optical images showed that significant morphological variations such as membrane blebbing occur in apoptotic cells over a time period of seconds. Acoustic measurements made one minute apart showed that the acoustic backscatter also changed with time (Fig. 11). The attenuation did not change during this measurement period. The ultrasound backscatter is primarily influenced by variations in structure, which are known to undergo rapid variations during apoptosis. Attenuation is primarily influenced by changes in bulk composition, for which variations occur on a longer timescale than structural variations. Therefore, we would expect to see rapid variations in the ultrasound backscatter but not attenuation during these measurements, as we observed in this study.

The normalized cross-correlation coefficient was used to quantify the activity observed during apoptosis (Fig. 10). The average correlation coefficient of treated but non-apoptotic cells was 0.93 ± 0.05, compared with 0.68 ± 0.17 for apoptotic cells. The lower correlation coefficient and higher standard deviation of apoptotic cells indicate extensive activity occurred within the cell over a time period of only seconds. This activity correlated to optical observations, where morphological variations in apoptotic cells were observed at the same timescales. Therefore the interior of the cell is also experiencing extensive structural changes during apoptosis that change the nature of the acoustic scattering, in addition to cellular membrane variations observed visually.

VI. Conclusion

We have shown, for the first time, high-resolution ultrasonic measurements of cells undergoing apoptosis. The ultrasonic properties, such as the thickness, sound velocity, acoustic impedance, density, bulk modulus, and attenuation of cells undergoing apoptosis were measured using time-resolved acoustic microscopy methods, and it was found only the thickness and attenuation increased during apoptosis. The other parameters remained similar within experimental error. Large changes in the scattering patterns occur when cells undergo apoptosis: although scattering occurs primarily at the cell,coupling fluid boundary for the non-responding cells, for cells undergoing apoptosis, scattering occurs throughout the entire cell, indicating large changes in intracellular structure. Finally, the acoustic measurements revealed that extensive activity is occurring within the cell during apoptosis, in addition to surface variations observed visually during a time period of only seconds.

Acknowledgments

The authors would like to acknowledge E. Weiss (Kibero GmbH, Germany), S. Brand (Fraunhofer Institute of Material Mechanics, Germany), and M. Rui and A. Worthington (Ryerson University, Canada) for technical support during this study.

References

[1] J. F. Kerr, A. H. Wyllie, and A. R. Currie, "Apoptosis: a basic biological phenomenon with wide-ranging implications in tissue kinetics," *Br. J. Cancer*, vol. 26, no. 4, pp. 239–257, 1972.

[2] A. H. Wyllie, J. F. R. Kerr, and A. R. Currie, "Cell death: The significance of apoptosis," *Int. Rev. Cytol.*, vol. 68, pp. 251–306, 1980.

[3] F. Kallel, R. J. Stafford, R. E. Price, R. Righetti, J. Ophir, and J. D. Hazle, "The feasibility of elastographic visualization of HIFU-induced thermal lesions in soft tissues," *Ultrasound Med. Biol.*, vol. 25, no. 4, pp. 641–647, 1999.

[4] G. I. Evan and K. H. Vousden, "Proliferation, cell cycle and apoptosis in cancer," *Nature*, vol. 411, no. 6835, pp. 342–348, 2001.

[5] B. Schutte and F. C. Ramaekers, "Molecular switches that govern the balance between proliferation and apoptosis," *Prog. Cell Cycle Res.*, vol. 4, pp. 207–217, 2000.

[6] F. T. Bosman, B. C. Visser, and J. Van Oeveren, "Apoptosis: Pathophysiology of programmed cell death," *Pathol. Res. Pract.*, vol. 192, no. 7, pp. 676–683, 1996.

[7] C. Haanen and I. Vermes, "Apoptosis: Programmed cell death in fetal development," *Eur. J. Obstet. Gynecol. Reprod. Biol.*, vol. 64, no. 1, pp. 129–133, 1996.

[8] H. J. M. Brady, *Apoptosis Methods and Protocols*. Totowa, NJ: Humana Press, 2004.

[9] C. B. Thompson, "Apoptosis in the pathogenesis and treatment of disease," *Science*, vol. 267, no. 5203, pp. 1456–1462, 1995.

[10] D. Hanahan and R. A. Weinberg, "The hallmarks of cancer," *Cell*, vol. 100, no. 1, pp. 57–70, 2000.

[11] Y. Tseng, T. P. Kole, and D. Wirtz, "Micromechanical mapping of live cells by multiple-particle-tracking microrheology," *Biophys. J.*, vol. 83, no. 6, pp. 3162–3176, 2002.

[12] M. Puig-De-Morales, M. Grabulosa, J. Alcaraz, J. Mullol, G. N. Maksym, J. J. Fredberg, and D. Navajas, "Measurement of cell microrheology by magnetic twisting cytometry with frequency domain demodulation," *J. Appl. Physiol.*, vol. 91, no. 3, pp. 1152–1159, 2001.

[13] E. Evans and A. Yeung, "Apparent viscosity and cortical tension of blood granulocytes determined by micropipet aspiration," *Biophys. J.*, vol. 56, no. 1, pp. 151–160, 1989.

[14] S. Felder and E. L. Elson, "Mechanics of fibroblast locomotion: Quantitative analysis of forces and motions at the leading lamellas of fibroblasts," *J. Cell Biol.*, vol. 111, no. 6, pt. 1, pp. 2513–2526, 1990.

[15] J. Sleep, D. Wilson, R. Simmons, and W. Gratzer, "Elasticity of the red cell membrane and its relation to hemolytic disorders: An optical tweezers study," *Biophys. J.*, vol. 77, no. 6, pp. 3085–3095, 1999.

[16] A. R. Bausch, F. Ziemann, A. A. Boulbitch, K. Jacobson, and E. Sackmann, "Local measurements of viscoelastic parameters of adherent cell surfaces by magnetic bead microrheometry," *Biophys. J.*, vol. 75, no. 4, pp. 2038–2049, 1998.

[17] H. W. Wu, T. Kuhn, and V. T. Moy, "Mechanical properties of L929 cells measured by atomic force microscopy: Effects of anticytoskeletal drugs and membrane crosslinking," *Scanning*, vol. 20, no. 5, pp. 389–397, 1998.

[18] M. C. Kolios, G. J. Czarnota, M. Lee, J. W. Hunt, and M. D. Sherar, "Ultrasonic spectral parameter characterization of apoptosis," *Ultrasound Med. Biol.*, vol. 28, no. 5, pp. 589–597, 2002.

[19] G. J. Czarnota, M. C. Kolios, J. Abraham, M. Portnoy, F. P. Ottensmeyer, J. W. Hunt, and M. D. Sherar, "Ultrasound imaging of apoptosis: High-resolution non-invasive monitoring of programmed cell death in vitro, in situ and in vivo," *Br. J. Cancer*, vol. 81, no. 3, pp. 520–527, 1999.

[20] A. S. Tunis, G. J. Czarnota, A. Giles, M. D. Sherar, J. W. Hunt, and M. C. Kolios, "Monitoring structural changes in cells with high-frequency ultrasound signal statistics," *Ultrasound Med. Biol.*, vol. 31, no. 8, pp. 1041–1049, 2005.

[21] M. C. Kolios, L. Taggart, R. E. Baddour, S. F. Foster, J. W. Hunt, G. J. Czarnota, and M. D. Sherar, "An investigation of backscatter power spectra from cells, cell pellets and microspheres," in *Proc. 2003 IEEE Int. Ultrasonics Symp.*, pp. 606–609.

[22] R. E. Baddour, M. D. Sherar, G. J. Czarnota, J. W. Hunt, L. Taggart, A. Giles, N. R. Farnoud, and M. C. Kolios, "High frequency ultrasound imaging of changes in cell structure including apoptosis," in *Proc. 2002 IEEE Int. Ultrasonics Symp.*, pp. 1639–1644.

[23] J. W. Hunt, A. E. Worthington, A. Xuan, M. C. Kolios, G. J. Czarnota, and M. D. Sherar, "A model based upon pseudo regular spacing of cells combined with the randomisation of the nuclei can explain the significant changes in high-frequency ultrasound signals during apoptosis," *Ultrasound Med. Biol.*, vol. 28, no. 2, pp. 217–226, 2002.

[24] G. J. Czarnota, M. C. Kolios, H. Vaziri, S. Benchimol, F. P. Ottensmeyer, M. D. Sherar, and J. W. Hunt, "Ultrasonic biomicroscopy of viable, dead and apoptotic cells," *Ultrasound Med. Biol.*, vol. 23, no. 6, pp. 961–965, 1997.

[25] G. Bao and S. Suresh, "Cell and molecular mechanics of biological materials," *Nat. Mater.*, vol. 2, no. 11, pp. 715–725, 2003.

[26] R. N. Johnston, A. Atalar, and J. Heiserman, "Acoustic microscopy: Resolution of subcellular detail," *Proc. Natl. Acad. Sci. USA*, vol. 76, no. 7, pp. 3325–3329, 1979.

[27] H. Lüers, K. Hillmann, J. Litniewski, and J. Bereiter-Hahn, "Acoustic microscopy of cultured cells. Distribution of forces and cytoskeletal elements," *Cell Biophys.*, vol. 18, no. 3, pp. 279–293, 1991.

[28] A. Kinoshita, S. Senda, K. Mizushige, H. Masugata, S. Sakamoto, H. Kiyomoto, and H. Matsuo, "Evaluation of acoustic properties of the live human smooth-muscle cell using scanning acoustic microscopy," *Ultrasound Med. Biol.*, vol. 24, no. 9, pp. 1397–1405, 1998.

[29] E. C. Weiss, P. Anastasiadis, G. Pilarczyk, R. M. Lemor, and P. V. Zinin, "Mechanical properties of single cells by high-frequency time-resolved acoustic microscopy," *IEEE Trans. Ultrason. Ferroelectr. Freq. Control*, vol. 54, no. 11, pp. 2257–2271, 2007.

[30] T. Kundu, J. Bereiter-Hahn, and I. Karl, "Cell property determination from the acoustic microscope generated voltage versus frequency curves," *Biophys. J.*, vol. 78, no. 5, pp. 2270–2279, 2000.

[31] P. V. Zinin, P. Anastasiadis, E. C. Weiss, and R. M. Lemor, "Variation of the sound attenuation inside HeLa cells during cell division using high-frequency time-resolved acoustic microscope," in *Proc. 2007 IEEE Int. Ultrasonics Symp.*, pp. 813–816.

[32] R. M. Lemor, E. C. Weiss, G. Pilarczyk, and P. V. Zinin, "Mechanical properties of single cells: Measurement possibilities using time-resolved scanning acoustic microscopy," in *Proc. 2004 IEEE Int. Ultrasonics Symp.*, pp. 622–629.

[33] J. A. Hildebrand and D. Rugar, "Measurement of cellular elastic properties by acoustic microscopy," *J. Microsc.*, vol. 134, no. 3, pp. 245–260, 1984.

[34] G. A. D. Briggs, J. Wang, and R. Gundle, "Quantitative acoustic microscopy of individual living human cells," *J. Microsc.*, vol. 172, no. 1, pp. 3–12, Oct. 1993.

[35] C. M. Daft and G. A. Briggs, "The elastic microstructure of various tissues," *J. Acoust. Soc. Am.*, vol. 85, no. 1, pp. 416–422, 1989.

[36] Y. Saijo, M. Tanaka, H. Okawai, and F. Dunn, "The ultrasonic properties of gastric cancer tissues obtained with a scanning acoustic microscope system," *Ultrasound Med. Biol.*, vol. 17, no. 7, pp. 709–714, 1991.

[37] Y. Saijo, M. Tanaka, H. Okawai, H. Sasaki, S. Nitta, and F. Dunn, "Ultrasonic tissue characterization of infarcted myocardium by scanning acoustic microscopy," *Ultrasound Med. Biol.*, vol. 23, no. 1, pp. 77–85, 1997.

[38] E. Maeva, F. Severin, C. Miyasaka, B. R. Tittmann, and R. G. Maev, "Acoustic imaging of thick biological tissue," *IEEE Trans. Ultrason. Ferroelectr. Freq. Control*, vol. 56, no. 7, pp. 1352–1358, 2009.

[39] E. M. Strohm and M. C. Kolios, "Measuring the mechanical properties of cells using acoustic microscopy," in *31st Annu. Int. Conf. IEEE EMBS*, 2009, pp. 6042–6045.

[40] O. Falou, J. C. Kumaradas, and M. C. Kolios, "Finite-element modelling of acoustic wave scattering from fluid, rigid and elastic objects," *Can. Acoust.–Acoust. Can.*, vol. 33, no. 3, pp. 84–85, 2005.

[41] O. Falou, R. E. Baddour, G. Nathanael, G. J. Czarnota, J. C. Kumaradas, and M. C. Kolios, "A study of high frequency ultrasound scattering from non-nucleated biological specimens," *J. Acoust. Soc. Am.*, vol. 124, no. 5, pp. EL278–EL283, 2008.

[42] O. Falou, J. C. Kumaradas, and M. C. Kolios, "Modelling high frequency acoustic backscatter response from nonnucleated biological specimens," *Can. Acoust.–Acoust. Can.*, vol. 36, no. 3, pp. 38–39, 2008.

[43] T. Kundu, *Ultrasonic Nondestructive Evaluation: Engineering and Biological Material Characterization*. Boca Raton, FL: CRC Press, 2004.

[44] A. Briggs, *Acoustic Microscopy*. New York, NY: Plenum Press, 1992.

[45] R. D. Weglein and R. G. Wilson, "Characteristic material signatures by acoustic microscopy," *Electron. Lett.*, vol. 14, pp. 352–354, Jun. 8, 1978.

[46] A. Atalar, "A physical model for acoustic signatures," *J. Appl. Phys.*, vol. 50, no. 12, pp. 8237–8239, 1979.

[47] A. Atalar, "An angular-spectrum approach to contrast in reflection acoustic microscopy," *J. Appl. Phys.*, vol. 49, no. 10, pp. 5130–5139, 1978.

[48] T. Kundu, J. Bereiter-Hahn, and K. Hillmann, "Measuring elastic properties of cells by evaluation of scanning acoustic microscopy

V(z) values using simplex algorithm," *Biophys. J.*, vol. 59, no. 6, pp. 1194–1207, 1991.
[49] M. Lemor, E. C. Weiss, G. Pilarczyk, and P. V. Zinin, "Measurements of elastic properties of cells using high-frequency time-resolved acoustic microscopy," in *Proc. 2003 IEEE Ultrasonics Symp.*, pp. 881–884.
[50] F. A. Duck, *Physical Properties of Tissue.* San Diego, CA: Academic Press, 1990.
[51] B. D. Ratner, J. Dyro, S. J. Grimnes, and F. J. Schoen, *Biomedical Engineering Desk Reference.* Oxford, UK: Academic Press, 2009.
[52] F. S. Foster, K. A. Harasiewicz, and M. D. Sherar, "A history of medical biological imaging with polyvinylidene fluoride (PVDF) transducers," *IEEE Trans. Ultrason. Ferroelectr. Freq. Control*, vol. 47, no. 6, pp. 1363–1371, 2000.
[53] *Measurement Specialties Piezo Film Sensors Technical Manual.* Measurement Specialties, Hampton, VA, 2006.
[54] D. E. Saunders, W. D. Lawrence, C. Christensen, N. L. Wappler, H. Ruan, and G. Deppe, "Paclitaxel-induced apoptosis in MCF-7 breast-cancer cells," *Int. J. Cancer*, vol. 70, no. 2, pp. 214–220, 1997.
[55] A. Miglietta, M. L. Panno, F. Bozzo, L. Gabriel, and C. Bocca, "Insulin can modulate MCF-7 cell response to paclitaxel," *Cancer Lett.*, vol. 209, no. 2, pp. 139–145, 2004.
[56] A. N. Shajahan, A. Wang, M. Decker, R. D. Minshall, M. C. Liu, and R. Clarke, "Caveolin-1 tyrosine phosphorylation enhances paclitaxel-mediated cytotoxicity," *J. Biol. Chem.*, vol. 282, no. 8, pp. 5934–5943, 2007.
[57] E. C. Weiss, R. M. Lemor, G. Pilarczyk, P. Anastasiadis, and P. V. Zinin, "Imaging of focal contacts of chicken heart muscle cells by high-frequency acoustic microscopy," *Ultrasound Med. Biol.*, vol. 33, no. 8, pp. 1320–1326, 2007.
[58] H. Kawai, "The piezoelectricity of polyvinylidene fluoride," *Jpn. J. Appl. Phys.*, vol. 8, no. 7, pp. 975–976, 1969.
[59] S. Brand, E. C. Weiss, R. M. Lemor, and M. C. Kolios, "High frequency ultrasound tissue characterization and acoustic microscopy of intracellular changes," *Ultrasound Med. Biol.*, vol. 34, no. 9, pp. 1396–1407, 2008.
[60] J. Kwong, H. L. Choi, Y. Huang, and F. L. Chan, "Ultrastructural and biochemical observations on the early changes in apoptotic epithelial cells of the rat prostate induced by castration," *Cell Tissue Res.*, vol. 298, no. 1, pp. 123–136, 1999.

Eric Strohm was born in Canada in 1976, and completed his B.Sc. Hons degree in physics at McMaster University in 1999. He subsequently completed his M.Sc. degree in physics at the University of British Columbia in 2001. He was employed as a member of the research staff at the Xerox Research Centre of Canada, Mississauga, Canada until 2007. In 2009, he completed his M.Sc. degree in biomedical physics from Ryerson University. He is currently employed as a research associate in the Biomedical Ultrasound Laboratory at Ryerson University in Toronto, Canada.

His research interests include imaging and characterization of biological cells and tissue, biological processes such as apoptosis and mitosis, and ultrasound contrast agents using high-frequency ultrasound and photoacoustic methods.

Gregory J. Czarnota was born in Canada in 1968 and completed a B.Sc. Hons degree in biochemistry at McMaster University in 1991. He subsequently completed his Ph.D. degree in the Department of Medical Biophysics at the University of Toronto in 1995. He completed postdoctoral studies in 1996 in that same department and then earned his M.D. degree from the University of Toronto in 2000. His F.R.C.P.C. specialization in Radiation Oncology was completed at the same university ending in 2005. He is currently a Clinician Scientist in the Department of Radiation Oncology, and in Imaging Research at Sunnybrook Health Sciences Centre in Toronto; an Assistant Professor in the Departments of Radiation Oncology and Medical Biophysics at the University of Toronto; and holds a CCO Research Chair in Experimental Therapeutics and Imaging.

His research interests include developing new ultrasound-based therapies for cancer treatment and imaging for detecting response efficacy.

Michael C. Kolios was born in Toronto, Canada, and moved to Greece at a young age, finishing his high school studies in Athens, Greece. He completed a B.Sc. Hons degree in physics, with a computer science minor, at the University of Waterloo in 1991. He subsequently completed his M.Sc. and Ph.D. degrees in the Department of Medical Biophysics at the University of Toronto in 1994 and 1998, respectively. In 1997, he joined the Department of Physics at Ryerson University, where he is currently an associate professor. He holds a Canada Research Chair in Biomedical Applications of Ultrasound and has been the recipient of numerous awards for his research and teaching.

His research interests include ultrasound /optical imaging and characterization of tissues and cells, high-frequency ultrasound imaging and spectroscopy, acoustic microscopy, ultrasound- and laser-based therapy, optical coherence tomography, and photoacoustic imaging.